



Emergence of ferroelectricity and spin-valley properties in two-dimensional honeycomb binary compounds

Domenico Di Sante,^{1,2,*} Alessandro Stroppa,^{1,†} Paolo Barone,¹ Myung-Hwan Whangbo,³ and Silvia Picozzi¹

¹*Consiglio Nazionale delle Ricerche (CNR-SPIN), Via Vetoio, I-67010 L'Aquila, Italy*

²*Department of Physical and Chemical Sciences, University of L'Aquila, Via Vetoio 10, I-67010 L'Aquila, Italy*

³*Department of Chemistry, North Carolina State University, Raleigh, North Carolina 27695-8204, USA*

(Received 2 January 2015; revised manuscript received 11 February 2015; published 6 April 2015)

By means of density functional theory calculations, we predict that several two-dimensional AB binary monolayers, where A and B atoms belong to group IV or III-V, are ferroelectric. Dipoles arise from the buckled structure, where the A and B ions are located on the sites of a bipartite corrugated honeycomb lattice with trigonal symmetry. We discuss the emerging valley-dependent properties and the coupling of spin and valley physics, which arise from the loss of inversion symmetry, and explore the interplay between ferroelectricity and Rashba spin-splitting phenomena. We show that valley-related properties originate mainly from the binary nature of AB monolayers, while the Rashba spin-texture developing around valleys is fully controllable and switchable by reversing the ferroelectric polarization.

DOI: [10.1103/PhysRevB.91.161401](https://doi.org/10.1103/PhysRevB.91.161401)

PACS number(s): 77.80.-e, 72.80.Ey, 73.21.-b, 71.15.Mb

Introduction. A wide range of modern electronic applications are based on the charge and spin degrees of freedom (DOF) of electrons. Two-dimensional (2D) atomic crystals with honeycomb lattice, such as graphene and molybdenum disulfide (MoS_2) monolayer, have recently been the object of intense research activities due to the additional valley DOF of carriers that might be useful in next-generation electronics applications [1–13]. In 2D semimetal graphene [1–4], the π and π^* bands linearly cross at K and $-K$ points of the hexagonal Brillouin zone (BZ), implying that charge carriers behave like massless Dirac fermions; at the same time, when spin-orbit coupling (SOC) is taken into account, the electrons experience opposite effective magnetic fields with equal magnitude at the K and $-K$ valleys (related by time-reversal symmetry). In principle, valley DOFs in graphene could be exploited for valley-dependent electronics and optoelectronics, but their control by electrical and optical means is difficult due to the inversion symmetry of the graphene crystal structure, preventing the appearance of valley-contrasting properties [12,13]. On the other hand, the 2D MoS_2 semiconductor [5–13] monolayer has no inversion symmetry and displays a direct band gap at the K and $-K$ valleys, enabling optical pumping of valley-polarized carriers by shining the monolayer with circularly polarized light [5,6].

Using first-principles calculations, Ciraci *et al.* investigated two-dimensional honeycomb structures of group-IV elements and their binary compounds as well as the compounds of group III-V elements [14]. It was found that buckled AB monolayers with trigonal symmetry (e.g., group IV binary monolayers SiGe, SiSn, GeSn and group III-V binary monolayers AlSb, GaP, GaAs, InP, InAs, InSb) [14], in which a trigonal sublattice of A ions is separated from that of B ions (Fig. 1(a) in Ref. [15]), are more stable with respect to a planar geometry. The tendency to a buckled geometry was explained in terms of the destabilization of

the π bonds in sp^2 hybridization due to the increase of the bond length between the two atoms A and B , as it happens in silicene and germanene compared to graphene [16]. Interestingly, silicene and germanene are expected to display valley-contrasting properties analogous to graphene as soon as the inversion symmetry is broken, e.g., by applying an external electric field [16]. Therefore other buckled honeycomb lattices are expected to display similar valley-dependent properties. Furthermore, in *buckled* trigonal structure, one can introduce a *sublattice pseudospin* ζ describing the binary layer DOF [12]: the pseudospin ζ up (down) refers to the state where the charge carrier is located in the upper (lower) layer, or equivalently in the A (B) sublattice. Therefore a pseudospin polarization would directly correspond to an electrical polarization. In fact, buckled AB monolayers have no inversion symmetry and actually belong to the *polar* space group $P3m_1$, with the polar axis perpendicular to the layer (Fig. 1(b) in Ref. [15]), possibly leading to a ferroelectric (FE) state; in addition to the emergence of valley-contrasting physics, therefore, they can also display a Rashba effect [17], which would likely be coupled to and controllable with the FE polarization. If this is the case, it would be possible to act on the spin DOFs of these valley-active systems by reversing the FE polarization of the monolayer [18].

From the experimental point of view, several top-down and bottom-up methods have been proposed and devised for synthesizing 2D materials, as reported in recent review papers [19,20]. Specifically, both silicene and germanene have been proven to exist as a monolayer when grown on selected metal substrates. Although bulk Si cannot form a layered phase like graphite, experiments of surface-assisted epitaxial growth show the presence of nanoribbons of silicene on Ag(110) [21] and 2D monolayers with buckled honeycomb structure on Ag(111) [22,23] and Ir(111) [24]. Similarly, successful attempts to grow 2D germanium sheets with a honeycomb structure on a platinum (111) and gold (111) template have been reported very recently [25,26]. As for binary compounds, to the best of our knowledge, no other 2D monolayers beside boron nitride have been synthesized yet [27], even though almost 2D nanoflakes of SiC with

*domenico.disante@spin.cnr.it

†alessandro.stroppa@aquila.infn.it

TABLE I. Buckling angle θ (deg), buckling height h (\AA), band gap E_g (eV), barrier height E_a (eV/fu), polarization P (10^{-12} C/m), and valence ΔE_{VB} and conduction ΔE_{CB} spin-splittings (meV) at the K point of buckled AB monolayers.

	θ (deg)	h (\AA)	E_g (eV)	E_a (eV/fu)	P (10^{-12} C/m)	ΔE_{VB} (meV)	ΔE_{CB} (meV)
SiGe	105.1	0.60	0.02	0.16	0.88	25.3	5.8
SiSn	105.4	0.72	0.98	0.23	4.22	79.8	38.0
GeSn	108.2	0.81	0.21	0.39	3.22	70.0	19.1
AlSb	105.2	0.68	1.43	0.14	7.82	20.0	50.8
GaP	101.3	0.44	2.16	0.05	9.24	7.4	5.3
GaAs	105.3	0.63	1.74	0.18	9.07	14.9	33.8
InP	102.4	0.53	1.33	0.07	11.45	21.0	10.4
InAs	105.9	0.70	0.87	0.22	11.10	36.4	45.8
InSb	107.5	0.83	0.69	0.30	8.30	57.2	100.9

thickness of the order of 1 nm have been obtained by means of solution-based exfoliation of SiC crystals [28]. On the other hand, recent theoretical calculations identified suitable substrates for the growth of 2D III-V compounds, proposing several lattice-matched substrates for their epitaxial growth, stabilization, and functionalization [29].

Results. Starting from the buckled compounds listed in Ref. [14], we have calculated the buckling heights h (\AA), band gaps E_g (eV), barrier heights E_a (eV per formula unit) estimated as the energy difference between the FE buckled structure and the paraelectric planar one, FE polarizations P (10^{-12} C/m) (see Ref. [15] for a discussion about the units) and spin-splittings ΔE_{VB} (ΔE_{CB}) (in meV) at the K point for valence (conduction) bands, see Table I. In this work, we follow previous theoretical studies [14] and assume that atoms A and B belong to the ordered bipartite lattice shown in Fig. 1(a) in Ref. [15], i.e., we neglect the role of disorder [30]; indeed, this effect would require a separate analysis, beyond the purpose of the present study. First, we note that if A and B atoms belong to the same group (i.e., IV group), the A - B bond is polar due to the electronegativity difference between A and B , since the electronegativity within a given family of elements decreases on going from the top to a lower period. On the other hand, when A and B atoms belong to III and V group, respectively, the electronegativity difference becomes even more pronounced (the electronegativity increasing from left to right along the period). The trigonal symmetry and the buckled honeycomb structure imply a local uniaxial dipole moment along the threefold rotation axis. By analogy with the Ising model for uniaxial ferromagnets, which is well known to display a phase transition even in the two-dimensional lattice [31], a FE phase transition is indeed possible, where the two symmetry-equivalent energy minima with opposite polarity are obtained by reversing the buckling angle. The estimated FE polarizations of the group IV binary AB monolayers are significantly large, with calculated typical values of the order of $1\text{--}4 \times 10^{-12}$ C/m, while the group III-V binary AB monolayers have a larger FE polarization, because of the larger electronegativity difference and larger dipole moment carried by each A - B bond. Typical values in this case are around 10×10^{-12} C/m. It is interesting to note that the calculated values for the estimated FE polarizations are always one order of magnitude larger than those measured in 2D freely suspended FE smectic-C films [32] and nematic monolayers [33], showing $P \sim 10^{-13}$ C/m. Evaluation of

Born effective charges Z^* confirms the estimated values of FE polarization, and, at the same time, provides an estimate of the depolarization field, which is expected to hinder the FE properties of thin films. The electrostatic energy of the depolarization field is proportional to the the square of Z^* and inversely proportional to the electronic polarizability of the material, i.e., $Z^{*2}/\epsilon_{zz}^\infty$ [34,35]; since the latter is almost constant for all the considered systems, i.e., $\epsilon_{zz}^\infty \sim 1$, while Z^* is significantly small (for the zz component of the charge tensor we calculate $Z_{zz}^* \sim 0.05e$ for group IV and $\sim 0.1e$ for group III-V binary AB monolayers), in our case, the depolarization field can be expected to be weaker than that preventing ferroelectricity in ultrathin films of ferroelectric perovskites [for reference, cubic perovskites typically have $Z^* \sim 5e$ and $\epsilon_{zz}^\infty \sim 6$], supporting the feasibility of stable FE distortions. Furthermore, the presence of stable phonon modes in the freestanding buckled geometry, reported in Ref. [14], strongly indicates that depolarizing fields do not suppress the tendency towards a polar ground state [36,37]. Inelastic electron excitations from a STM tip could be used to switch between the two FE phases, as recently proposed for bistable molecular switches [38,39]. It should be pointed out that our study applies only to freestanding monolayer, since the presence of a substrate could lead to energetically nonequivalent FE states in real device applications.

We discuss then the electronic band structures of a representative example, GeSn, calculated without and with SOC and shown in Figs. 1(a) and 1(b). Band structures for all the other compounds are displayed in Fig. 2 in Ref. [15]. The band gap opens at the K point, where both the valence (VB) and conduction (CB) bands are split by SOC, as highlighted in Fig. 1(c). It is also clear from Fig. 1(c) that electrons around the K valley feel a strong Zeeman-like magnetic field, which is responsible for a valley-dependent out-of-plane spin polarization both in the VB and in the CB [9]. The same holds for the $-K$ valley. Due to the time-reversal symmetry, the system remains overall nonmagnetic, with opposite out-of-plane spin polarization at time-reversed K and $-K$ points, as clearly shown in Figs. 1(e) and 1(g). Therefore the considered buckled FE monolayers show coupled spin and valley physics, thus possibly allowing for spin and valley control similar to layered transition-metal dichalcogenides. As for MoS_2 and other group-VI dichalcogenides, the valley Hall effect should be accompanied by a spin Hall effect for both the electron and hole-doped systems, whose robustness can be deduced by the

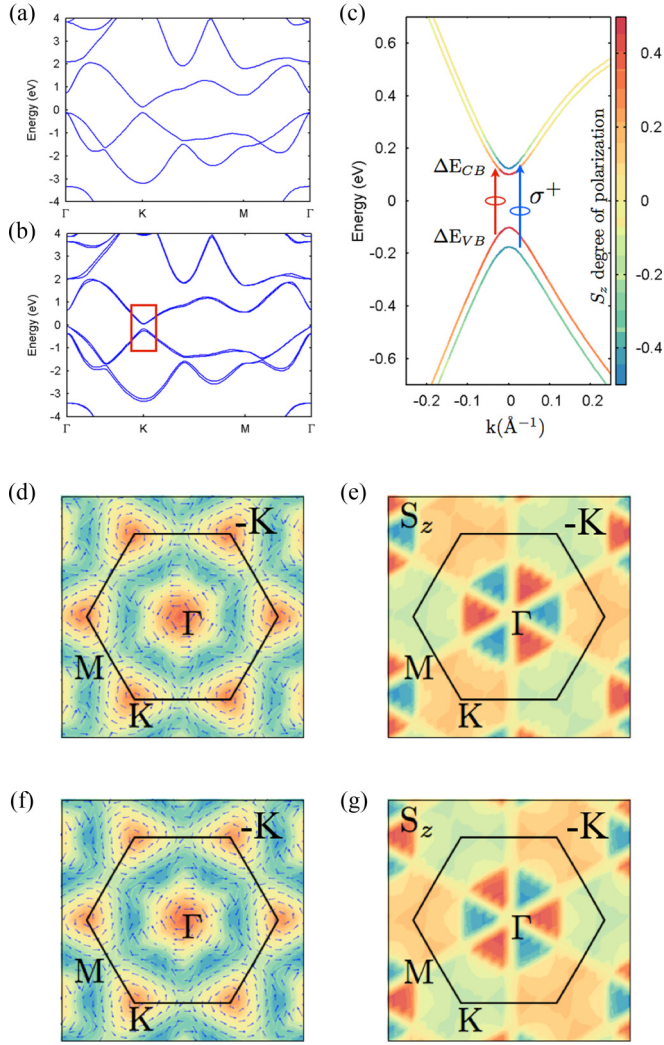


FIG. 1. (Color online) (a) Band structures along the 2D hexagonal Brillouin zone (BZ) (a) without and (b) with SOC. In (b) the red panel is an eye guide for the zoomed-in view in (c), where low-energy bands around the Fermi level in the vicinity of K are reported. The color scale refers to the out-of-plane S_z spin polarization, while the red and blue arrows, referring to positive and negative S_z spin-component gaps, respectively, denote the valley and spin optical transition selection rules for circularly polarized light needed at K for optical interband excitations. (d) and (e) In-plane and out-of-plane spin textures of the upper and (f) and (g) lower spin-split VBs for the whole BZ. In (d) and (f), the color coding refers to the wave-vector-dependent energy highlighting the C_{3v} symmetry, while the color scale for the S_z degree of polarization in (e) and (g) is consistent with (c).

expected long relaxation time of spin and valley indices [13]. The spin textures of the two spin-split VBs calculated for the whole BZ are presented in Figs. 1(d) and 1(g). The typical Rashba spin patterns are clearly observed around K and $-K$ valleys, with the in-plane spin components rotating clockwise or counterclockwise in spin-split bands, as shown in Figs. 1(d) and 1(f) for upper and lower VBs. Interestingly, while the out-of-plane spin components show opposite polarizations at time-reversed valleys, the in-plane spin components display the same chirality at K and $-K$ points in a single VB; both

the Rashba-like chirality and the valley-dependent magnetic moments appear then to be reversed in the other spin-split VB. A similar behavior is found in the spin-split CBs, while the VB maximum (VBM) and CB minimum (CBM) show same chiralities and out-of-plane polarization direction. When the FE polarization is switched by reversing the buckling, the in-plane spin-texture chiralities are fully reversed, suggesting possibilities to control the Rashba effect by exploiting the FE properties of binary monolayers. On the other hand, the out-of-plane spin polarization remains exactly the same in opposite FE states. Interestingly, the valley-dependent spin polarization survives even when the buckling is completely suppressed as in the flat graphenelike structure, as a consequence of the noncentrosymmetric, albeit nonpolar, character of the planar honeycomb structure with binary composition.

To understand the origin of this exotic spin and valley physics, and its interplay with the intrinsic FE polarization in buckled trigonal monolayers, we now investigate the microscopic mechanisms underlying the low-energy properties around the Fermi level at the K and $-K$ valleys. In the absence of buckling ($\theta = \pi/2$) and SOC, the low-energy effective Hamiltonian around the K point describing low-energy states with mainly p_z character reads

$$H_K^{(0)} = -m\zeta_z + v_F(\tau k_x \zeta_x - k_y \zeta_y), \quad (1)$$

where ζ is the sublattice pseudospin transforming like Pauli matrices, $\tau = \pm 1$ is a valley index for K points, v_F is the Fermi velocity, and the first “mass” term originates from the different ions located in A and B sublattices. Contrary to the case of graphene, silicene and other group-IV binary monolayers [3,40–42], the additional mass term leads to an intrinsic gap in the energy spectrum, which opens at the Dirac point (the effective parameters are estimated in a tight-binding framework and given in Ref. [15]). The VBs and CBs remain spin degenerate, as sketched in Fig. 2(a) for VBs. When SOC is turned on in the planar structure ($\theta = \pi/2$), additional terms appear in the effective Hamiltonian (1), namely,

$$H_K^{(1)} = H_K^{(0)} - \tau \sigma_z \lambda_{so}^+ \zeta_z - \tau \sigma_z \lambda_{so}^-, \quad (2)$$

where $\lambda_{so}^\pm = (\lambda_{so}^A \pm \lambda_{so}^B)/2$ are effective material-dependent parameters arising from the interplay of atomic SOC constants $\xi_{A/B}$, local orbital energies $\Delta_{A/B}$, and hopping integrals $V_{sp\sigma}$, $V_{pp\sigma}$, and $V_{pp\pi}$, which in turn depend on geometrical factors such as the buckling angle θ (see Ref. [15]). The presence of SOC, therefore, introduces an effective Zeeman-like valley-dependent magnetic field $B^{\text{eff}} = -\tau \lambda_{so}^-$, which removes the spin-degeneracy without mixing spin-up and spin-down states, leading to spin-split VBs and CBs with energies $E_\sigma = -\sigma \tau \lambda_{so}^- \pm \sqrt{(m + \sigma \tau \lambda_{so}^+)^2 + v_F^2 k^2}$ and a net out-of-plane spin polarization at the K valleys, as sketched in Fig. 2(b). The VB and CB spin-splittings are listed in Table I for all considered binary monolayers, and shown in Fig. 1(c) for the representative case of GeSn. Additionally, the mass term acquires a spin-valley-sublattice contribution $\tau \sigma_z \zeta_z \lambda_{so}^+$, which indeed guarantees the coupling between the spin and valley physics. Interestingly, the additional coupling terms experienced by a given sublattice originate from the atomic SOC of the other sublattice mediated by the hopping interactions—in fact, carriers in the A sublattice feel the atomic

SOC of B ions through the term $\lambda_{so}^B \sigma_z$, and vice versa. This is reflected in the different size of spin-splitting gaps in VBs and CBs. As shown in Fig. 1(c) for the representative case of GeSn, the spin splitting is larger at VBs rather than at CBs, despite the fact that VBs and CBs show predominant Ge and Sn characters, respectively, as a consequence of the larger electronegativity of Ge. Naïvely, one would expect a larger spin-splitting at CBs than at VBs, since the atomic SOC constant of Sn is larger than that of Ge, $\xi_{Sn} > \xi_{Ge}$ [43]. Indeed, the opposite is observed, since carriers with a predominant Ge character experience the SOC-induced interaction coming from the Sn ions, and vice versa. The same holds for all other compounds, as can be inferred looking at values reported in Table I. It is important to stress that such spin-splitting effects arise uniquely from the binary composition of the monolayers, implying $\lambda_{so}^- \neq 0$. The spin-valley coupling, emerging already in the planar noncentrosymmetric binary monolayer, is therefore independent of the buckling distortion; in fact, the $\lambda_{so}^{A/B}$ are even functions of the buckling angle θ , implying that valley-contrasting properties such as the out-of-plane spin polarization are not expected to qualitatively change under FE distortions. Furthermore, since the valley-dependent coupling terms do not mix the spin-up and spin-down components, σ_z remains a good quantum number, analogously to what happens in MoS₂ monolayers.

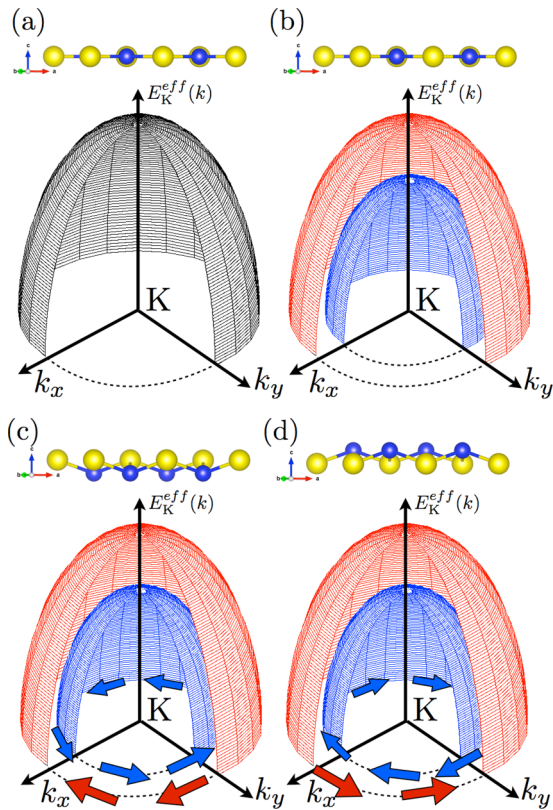


FIG. 2. (Color online) (a) and (b) Valence bands (VBs) at the valley without (a) and with (b) SOC. Red and blue colored bands in (b)–(d) refer to the presence of positive and negative out-of-plane spin polarizations, respectively. (c) and (d) VBs and relative in-plane spin-texture for positive and negative buckling.

One can easily evaluate the Berry curvature of the Bloch electrons, associated with the valley and spin Hall effect:

$$\Omega_{\sigma} = \mp \tau \frac{2v_F^2(m + \sigma\tau\lambda_{so}^+)}{[v_F^2k^2 + (m + \sigma\tau\lambda_{so}^+)^2]^{3/2}}, \quad (3)$$

where the \mp sign refers to CB and VB, respectively, as well as the coupling strength with optical fields of $\hat{\sigma}^{\pm}$ circular polarization:

$$|\mathcal{P}_{\pm}(k)|^2 \propto \left(1 \pm \tau \frac{m + \sigma\tau\lambda_{so}^+}{\sqrt{v_F^2k^2 + (m + \sigma\tau\lambda_{so}^+)^2}} \right), \quad (4)$$

which display the same form found for MoS₂ monolayers, leading to similar expectations about the robustness of (valley and spin) Hall physics and optoelectronic effects [13]. In particular, the Berry curvature shows opposite sign in different valleys, while the interband optical transitions are found to be uniquely coupled with a $\hat{\sigma}^+$ ($\hat{\sigma}^-$) circularly polarized optical field at the K ($-K$) valley, the valley optical selection rules being also spin-dependent as shown in Fig. 1(c). It is also clear from Eqs. (3) and (4) that the strength of such spin-valley physics is mainly governed by the spin-valley-sublattice coupling parametrized by λ_{so}^+ , even though the valley-contrasting spin splitting of both VBs and CBs is due to the effective magnetic field $\tau\lambda_{so}^-$.

When ferroelectricity sets in, lowering the trigonal symmetry from C_{3h} to C_{3v} and leading to a finite buckling $\theta \neq \pi/2$, an intrinsic Rashba term must be added in the effective Hamiltonian (2), namely,

$$H_K^{(2)} = H_K^{(1)} - (\lambda_R^+ \zeta_z + \lambda_R^-)(k_y \sigma_x - k_x \sigma_y), \quad (5)$$

where $\lambda_R^{\pm} = (\lambda_R^A \pm \lambda_R^B)/2$, and $\lambda_R^{A/B}$ is a complex material-dependent parameter which is odd under the switching of the buckling angle (see Ref. [15]). This Rashba coupling term gives rise to in-plane circularly rotating spin-texture around each K valley, with opposite chiralities at spin-split VBs (CBs) as shown in Fig. 2(c), while substantially not affecting the out-of-plane spin polarization. Neglecting λ_R^- for the sake of simplicity, the expectation value for in-plane spin polarizations reads $\langle \sigma_x \rangle \propto -\lambda_R^+ k_y$ and $\langle \sigma_y \rangle \propto \lambda_R^+ k_x$ for the VBM and CBM (the overall chirality being fully reversed in the VBM-1 and CBM+1 branches), i.e., typical Rashba-like behavior, which appears to be valley-independent, in agreement with our DFT calculations. Since $\lambda_R^{A/B}$ is an odd function of the buckling angle with respect to planar structure $\theta = \pi/2$, the buckling reversal, i.e., the switching of the ferroelectric polarization, leads to a complete reversal of the in-plane Rashba spin-texture chirality only, while the VBs and CBs preserve their out-of-plane spin-polarization, as schematically shown in Figs. 2(c)–2(d). This behavior perfectly agrees with our first-principles calculations, since its origin lies in the opposite θ dependence of spin-valley ($\lambda_{so}^{A/B}$) and intrinsic Rashba ($\lambda_R^{A/B}$) coupling constants at, and around, the K point (note that $\lambda_R^{A/B} \neq 0$ only when $\theta \neq \pi/2$ and the k vector differs from K [41]). It is worthwhile to notice that, although the Rashba-like coupling term causes a mixing of spin-up and spin-down states, the valley physics appears to be robust

to buckling distortion. In fact, the Berry curvature has been evaluated from first-principles for the representative GeSn with buckled honeycomb structure, and it has been found to display opposite sign at K and $-K$ valleys, as shown in Fig. 3 in Ref. [15].

Conclusions. In this work, we predict a spontaneous FE polarization in freestanding buckled group IV and group III-V binary monolayers with trigonal symmetry. Unlike the case of graphene, silicene, germanene, and other single atomic type monolayers, the presence of a diatomic basis that breaks the inversion symmetry—even in the planar geometry—leads to the emergence of Zeeman-like spin-split bands with coupled spin-valley physics analogous to the MoS₂ case. At the same time, it is mainly responsible for the onset of the FE phase when the honeycomb lattice buckles, allowing for an electrically controllable Rashba-like spin-texture around the K valleys, whose chirality is locked to the polarization direction and therefore fully reversible upon FE switching.

Such Rashba split bands can be effectively detected by spin-resolved spectroscopic techniques, and the process of hole and electron injection allows for the engineering of two-dimensional spin field-effect-transistors (FETs) [18]. Even though the spin-valley and Rashba phenomenologies appear to be substantially decoupled, our work suggests a route towards the integration of valleytronic and spintronic features in FE multivalley materials, opening unforeseen possibilities in the exciting world of spintronics. Currently, the growth of these 2D monolayers on a suitable substrate is difficult, and the effect of the substrate has been only recently addressed [29].

The authors are thankful to the HPC Center of NCSU for computing resources. A.S. acknowledges the CNR STM program (AMMCNT-CNR0026336) supporting the visit at IFW Leibniz Institute (Germany) where this project was conceived and started.

-
- [1] A. Rycerz, J. Tworzydo, and C. W. J. Beenakker, Valley filter and valley valve in graphene, *Nat. Phys.* **3**, 172 (2007).
- [2] D. Xiao, W. Yao, and Q. Niu, Valley-contrasting physics in graphene: Magnetic moment and topological transport, *Phys. Rev. Lett.* **99**, 236809 (2007).
- [3] A. H. Castro Neto, F. Guinea, N. M. R. Peres, K. S. Novoselov, and A. K. Geim, The electronic properties of graphene, *Rev. Mod. Phys.* **81**, 109 (2009).
- [4] M.-K. Lee, N.-Y. Lue, C.-K. Wen, and G. Y. Wu, Valley-based field-effect transistors in graphene, *Phys. Rev. B* **86**, 165411 (2012).
- [5] H. Zeng, J. Dai, W. Yao, D. Xiao, and X. Cui, Valley polarization in MoS₂ monolayers by optical pumping, *Nat. Nanotechnol.* **7**, 490 (2012).
- [6] K. F. Mak, K. He, J. Shan, and T. F. Heinz, Control of valley polarization in monolayer MoS₂ by optical helicity, *Nat. Nanotechnol.* **7**, 494 (2012).
- [7] T. Cao, G. Wang, W. Han, H. Ye, C. Zhu, J. Shi, Q. Niu, P. Tan, E. Wang, B. Liu *et al.*, Valley-selective circular dichroism of monolayer molybdenum disulphide, *Nat. Commun.* **3**, 887 (2012).
- [8] K. Behnia, Condensed-matter physics: Polarized light boosts valleytronics, *Nat. Nanotechnol.* **7**, 488 (2012).
- [9] H. Yuan, M. S. Bahramy, K. Morimoto, S. Wu, K. Nomura, B.-J. Yang, H. Shimotani, R. Suzuki, M. Toh, C. Kloc *et al.*, Zeeman-type spin splitting controlled by an electric field, *Nat. Phys.* **9**, 563 (2013).
- [10] C. Mai, A. Barrette, Y. Yu, Y. G. Semenov, K. W. Kim, L. Cao, and K. Gundogdu, Many-body effects in valleytronics: Direct measurement of valley lifetimes in single-layer MoS₂, *Nano Lett.* **14**, 202 (2014).
- [11] K. F. Mak, K. L. McGill, J. Park, and P. L. McEuen, The valley hall effect in MoS₂ transistors, *Science* **344**, 1489 (2014).
- [12] X. Xu, W. Yao, D. Xiao, and T. F. Heinz, Spin and pseudospins in layered transition metal dichalcogenides, *Nat. Phys.* **10**, 343 (2014).
- [13] D. Xiao, G.-B. Liu, W. Feng, X. Xu, and W. Yao, Coupled spin and valley physics in monolayers of MoS₂ and other group-VI dichalcogenides, *Phys. Rev. Lett.* **108**, 196802 (2012).
- [14] H. Şahin, S. Cahangirov, M. Topsakal, E. Bekaroglu, E. Akturk, R. T. Senger, and S. Ciraci, Monolayer honeycomb structures of group-IV elements and III-V binary compounds: First-principles calculations, *Phys. Rev. B* **80**, 155453 (2009).
- [15] See Supplemental Material at <http://link.aps.org/supplemental/10.1103/PhysRevB.91.161401> for additional details on structural and electronic properties, as well as model Hamiltonian analysis.
- [16] M. Ezawa, Spin valleytronics in silicene: Quantum spin Hall-quantum anomalous Hall insulators and single-valley semimetals, *Phys. Rev. B* **87**, 155415 (2013).
- [17] E. I. Rashba, Properties of semiconductors with an extremum loop. 1. Cyclotron and combinational resonance in a magnetic field perpendicular to the plane of the loop, *Sov. Phys. Solid State* **2**, 1109 (1960).
- [18] D. Di Sante, P. Barone, R. Bertacco, and S. Picozzi, Electric control of the giant rashba effect in bulk GeTe, *Adv. Mater.* **25**, 509 (2013).
- [19] S. Z. Butler, S. M. Hollen, L. Cao, Y. Cui, J. A. Gupta, H. R. Gutierrez, T. F. Heinz, S. S. Hong, J. Huang, A. F. Ismach *et al.*, Progress, challenges, and opportunities in two-dimensional materials beyond graphene, *ACS Nano* **7**, 2898 (2013).
- [20] S. Balendhran, S. Walia, H. Nili, S. Sriram, and M. Bhaskaran, Elemental analogues of graphene: Silicene, germanene, stanene, and phosphorene, *Small* **11**, 640 (2015).
- [21] B. Aufray, A. Kara, S. Vizzini, H. Oughaddou, C. Léandri, B. Ealet, and G. Le Lay, Graphene-like silicon nanoribbons on Ag(110): A possible formation of silicene, *Appl. Phys. Lett.* **96**, 183102 (2010).
- [22] P. Vogt, P. De Padova, C. Quaresima, J. Avila, E. Frantzeskakis, M. C. Asensio, A. Resta, B. Ealet, and G. Le Lay, Silicene: Compelling experimental evidence for graphene-like two-dimensional silicon, *Phys. Rev. Lett.* **108**, 155501 (2012).
- [23] B. J. Feng, Z. J. Ding, S. Meng, Y. Yao, X. He, P. Cheng, L. Chen, and H. Wu, Evidence of silicene in honeycomb structures of silicon on Ag(111), *Nano Lett.* **12**, 3507 (2012).

- [24] L. Meng, Y. Wang, L. Zhang, S. Du, R. Wu, L. Li, Y. Zhang, G. Li, H. Zhou, W. A. Hofer *et al.*, Buckled silicene formation on Ir(111), *Nano Lett.* **13**, 685 (2013).
- [25] L. Li, S.-Z. Lu, J. Pan, Z. Qin, Y.-Q. Wang, Y. Wang, G.-Y. Cao, S. Du, and H.-J. Gao, Buckled germanene formation on Pt(111), *Adv. Mater.* **26**, 4820 (2014).
- [26] M. E. Dávila, L. Xian, S. Cahangirov, A. Rubio, and G. Le Lay, Germanene: A novel two-dimensional germanium allotrope akin to graphene and silicene, *New J. Phys.* **16**, 095002 (2014).
- [27] P. Miró, M. Audiffred, and T. Heine, An atlas of two-dimensional materials, *Chem. Soc. Rev.* **43**, 6537 (2014).
- [28] S. S. J. Lin, Previous Article Next Article Table of Contents Light-Emitting two-dimensional ultrathin silicon carbide, *Phys. Chem. C* **116**, 3951 (2012).
- [29] A. K. Singh, H. L. Zhuang, and R. G. Hennig, *Ab initio* synthesis of single-layer III-V materials, *Phys. Rev. B* **89**, 245431 (2014).
- [30] D. Di Sante, P. Barone, E. Plekhanov, S. Ciuchi, and S. Picozzi, Robustness against disorder of relativistic spectral properties in chalcogenide alloys, [arXiv:1407.2064](https://arxiv.org/abs/1407.2064).
- [31] L. Onsager, Crystal Statistics. I. A Two-Dimensional Model with an Order-Disorder Transition, *Phys. Rev.* **65**, 117 (1944).
- [32] C. Rosenblatt, R. Pindak, N. A. Clark, and R. B. Meyer, Freely suspended ferroelectric liquid-crystal films: Absolute measurements of polarization, elastic constants, and viscosities, *Phys. Rev. Lett.* **42**, 1220 (1979).
- [33] Y. Tabe, T. Yamamoto, I. Nishiyama, M. Yoneya, and H. Yokoyama, Ferroelectric nematic monolayer, *Jpn. J. Appl. Phys.* **42**, L406 (2003).
- [34] W. Zhong, R. D. King-Smith, and D. Vanderbilt, Giant LO-TO splittings in perovskite ferroelectrics, *Phys. Rev. Lett.* **72**, 3618 (1994).
- [35] K. F. Garrity, K. M. Rabe, and D. Vanderbilt, Hyperferroelectrics: Proper Ferroelectrics with Persistent Polarization, *Phys. Rev. Lett.* **112**, 127601 (2014).
- [36] S. N. Shirodkar and U. V. Waghmare, Emergence of ferroelectricity at a metal-semiconductor transition in a 1T monolayer of MoS₂, *Phys. Rev. Lett.* **112**, 157601 (2014).
- [37] Na Sai, C. J. Fennie, and A. A. Demkov, Absence of Critical Thickness in an Ultrathin Improper Ferroelectric Film, *Phys. Rev. Lett.* **102**, 107601 (2009).
- [38] Q. Fu, Y. Luo, J. Yang, and J. Hou, Understanding the concept of randomness in inelastic electron tunneling excitations, *Phys. Chem. Chem. Phys.* **12**, 12012 (2010).
- [39] N. Pavliček, B. Fleury, M. Neu, J. Niedenführ, C. Herranz-Lancho, M. Ruben, and J. Repp, Atomic force microscopy reveals bistable configurations of dibenzo[a,h]thianthrene and their interconversion pathway, *Phys. Rev. Lett.* **108**, 086101 (2012).
- [40] S. Konschuh, M. Gmitra, and J. Fabian, Tight-binding theory of the spin-orbit coupling in graphene, *Phys. Rev. B* **82**, 245412 (2010).
- [41] C.-C. Liu, H. Jiang, and Y. Yao, Low-energy effective hamiltonian involving spin-orbit coupling in silicene and two-dimensional germanium and tin, *Phys. Rev. B* **84**, 195430 (2011).
- [42] N. D. Drummond, V. Zólyomi, and V. I. Fal'ko, Electrically tunable band gap in silicene, *Phys. Rev. B* **85**, 075423 (2012).
- [43] K. Wittel and R. Manne, Atomic spin-orbit interaction parameters from spectral data for 19 elements, *Theoret. Chim. Acta (Berl.)* **33**, 347 (1974).